Pergamon

Acta mater. Vol. 46, No. 4, pp. 1283–1295, 1998

Published by Elsevier Science Ltd
Printed in Great Britain

PII: S1359-6454(97)00298-X

1359-6454/98 $19.00 + 0.00

INFRARED JOINING OF TiAl INTERMETALLICS USING Ti–15Cu–15Ni FOIL—I. THE MICROSTRUCTURE MORPHOLOGIES OF JOINT INTERFACES

S. J. LEE[1], S. K. WU[1] and R. Y. LIN[2]

[1]Institute of Materials Science and Engineering, National Taiwan University, Taipei, Taiwan 106, Republic of China and [2]Department of Materials Science and Engineering, University of Cincinnati, Cincinnati, OH 45221, U.S.A.

(Received 4 April 1997; accepted 25 July 1997)

Abstract—Infrared joining of TiAl using Ti–15Cu–15Ni(wt%) foil as brazing filler metal was investigated at the temperature range of 1100°C ~ 1200°C for 30 ~ 60 s in a flowing argon environment. All the cross-sectioned microstructures at joint interfaces show distinct multilayered structures which were mainly formed by isothermal solidification and following solid-state interdiffusion during joining. The inward diffusion of Al atoms from the TiAl base metal is found to be the main controlling factor pertaining to the microstructural evolution of the joint interface. Seven characteristic zones can be distinguished in the joint. The locus of each specific zone shows a continuously or smoothly varying interval in the diffusion-path diagram and corresponds to one of the stable phases existing at the joining temperature. Experimental results show that the diffusion path of the joint interface at 1150°C are: (a) γ-TiAl/α-Ti/α + β/β-Ti/Residual liquid-phase for holding 30 s and (b) γ-TiAl/α-Ti/α_2-Ti_3Al/β-Ti/Res idual liquid-phase for holding 60 s. The observed joint microstructures are obtained from the phase transformation of these well-established high-temperature phases through rapid cooling to room temperature.

1. INTRODUCTION

Titanium-aluminides have low densities, high melting temperatures, good elevated-temperature strength and modulus retention, and excellent creep properties [1–4]. However, they suffer from low ductility and toughness at ambient temperatures which, along with poor formability, appears to be the single most serious obstacle to their full utilization [1]. By directly joining titanium-aluminide components into an integral structure, some problems in formation could be eliminated effectively. Thus, appropriate joining techniques are indispensable for the practical utilization of this material in elevated-temperature structural applications.

Welding, diffusion-bonding and brazing are three joining techniques which have been commonly applied in industry. Electron beam welding in TiAl was studied by Patterson *et al.* [5] who reported that welding cracks cannot easily be avoided. Baeslack *et al.* have done weldability studies on different titanium aluminide alloys [6, 7]. Optimum weld structure and properties can be obtained by properly controlling the weld cooling rates. Concerning diffusion-bonding, Nakao *et al.* [8] investigated the diffusion bonding of Ti–52Al. Yan and Wallach [9] studied the solid-state diffusion bonding and transient-liquid-phase bonding of Ti–48Al. Very recently, Cam *et al.* [10] investigated the solid-state diffusion bonding of TiAl carried out under different bonding temperatures within the superplastic temperature range of 925 ~ 1100°C. Although solid-bonds with rather good joint properties can be acquired by diffusion bonding, the long processing time and the high corresponding operation/installation costs may render this joining method useless for practical applications, especially for joining large-sized workpieces.

On the other hand, brazing, as an effective joining process, can offer many advantages over other joining processes such as a relatively low joining temperature, the possibility of making many joints at one pass, dissimilar-material joining, complex structure joining, high precision and better joint properties [11]. For joining titanium-aluminides, conventional furnace brazing with slow heating and cooling rates does not easily provide desirable joint properties due to its long elevated-temperature heat-history. This may be the reason why only a few studies on brazing of titanium-aluminides have been reported [12, 13].

During the past few years, a rapid isothermal process (RIP) technique has apparently been developed and widely applied in the electronic industry [14]. Infrared joining, one of the RIPs, can offer a very quick and cost-effective method for joining advanced materials [12]. The infrared joinings of TiAl have been studied by Lin *et al.* using Ti–15Cu–15Ni[13] and Al–Si[12] foils as brazing filler-metals. The multilayered microstructures of joint interfaces and the compressive-shear joint strength

of about 170–220 MPa were reported, but the reasons why or how those multilayered structures formed have still not been clarified.

Since joint properties are strongly dependent on microstructures, it is important that the microstructural evolution in the joint interface can be elucidated. The aim of this study was to investigate the microstructural evolution of brazed interfaces during infrared joining by using Ti–15Cu–15Ni as the filler metal. In Part I of this study, using the Ti–Al–Ni(Cu) pseudo-ternary diffusion-path diagrams, the high-temperature phases of the characteristic zones shown in the observed multilayered structures of joint interfaces can be identified. Their phase transformations during rapid cooling from the infrared joining temperature will also be discussed. In Part II of this study, the time-dependent microstructural evolution at a specific joining temperature and the effects of the joining temperature on the microstructural evolution will be discussed in detail. The multiphase diffusion theories [15–17] in binary and ternary solid-state systems are used to discuss the microstructural evolution and its relationships to the phase diagrams used in this study.

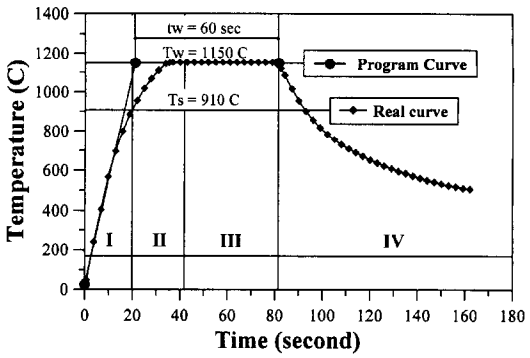

Fig. 1. The real temperature vs. real time chart of sample #2. The entire joining process can be divided into four main stages: (I)heating, (II)dissolution, (III)isothermal solidification and (IV)cooling stages. T_w, T_s and t_w is the joining temperature, the solidus of Ticuni filler-metal and the programmer setting holding time, respectively.

2. EXPERIMENTAL PROCEDURES

A conventional tungsten vacuum arc melting technique was employed to prepare the $Ti_{50}Al_{50}$ (at.%) alloy. The as-melted button was homogenized at 1200°C in a 7×10^{-5} torr vacuum furnace for 50 h and then followed by furnace cooling. The homogenized button was cut into $10 \times 8 \times 3$ mm and $5 \times 8 \times 3$ mm specimens by wire-cutting for subsequent infrared joining. These specimens were

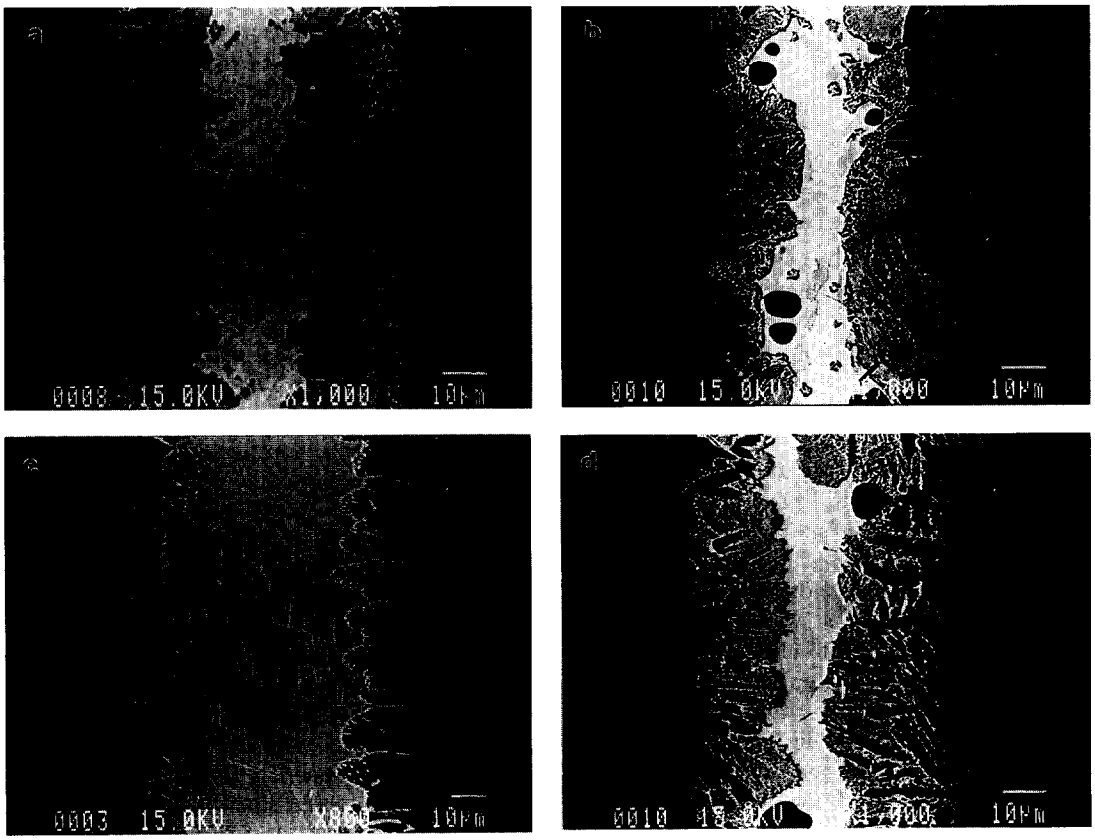

Fig. 2. (a) ~ (d) are the back-scattering electron images (BEIs) of joint interfaces for specimens (a) #1: 1150°C × 30s, (b) #2: 1150°C × 60s, (c) #3: 1100°C × 30s and (d) #4: 1200°C × 30s, respectively.

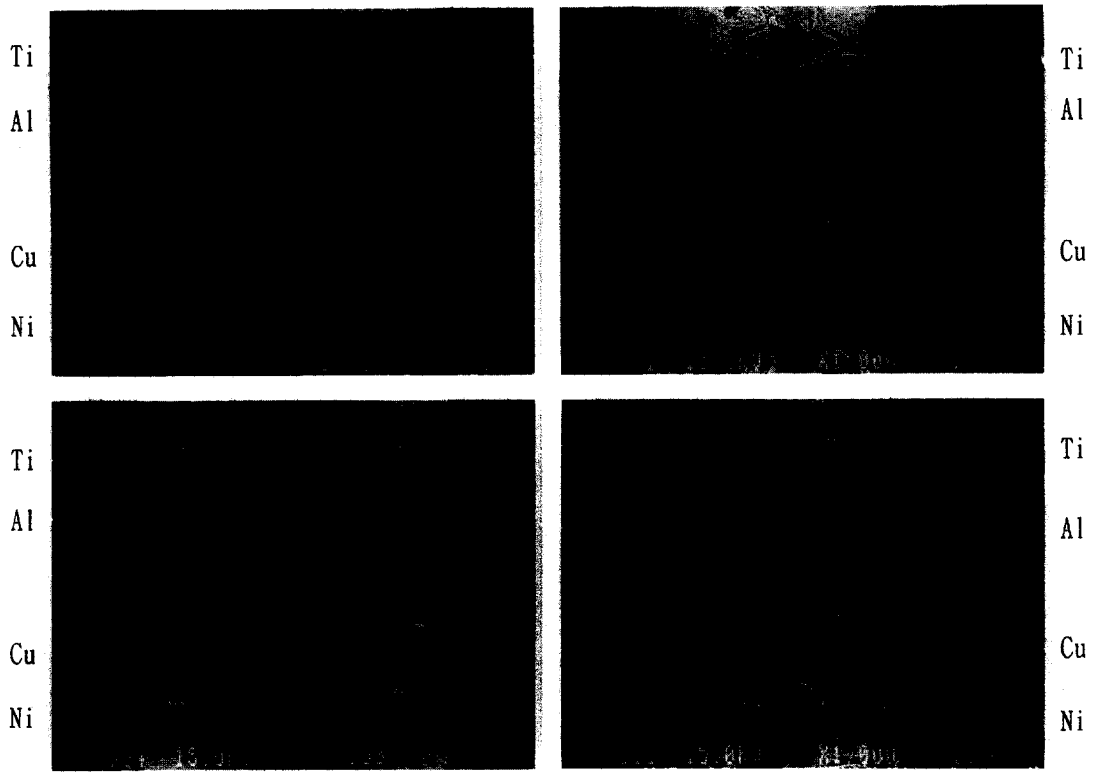

Fig. 3. (a) ~ (d) are the secondary electron images (SEIs) with Ti, Al, Cu and Ni LSPs of joint interfaces for specimens (a) #1: 1150°C × 30s, (b) #2: 1150°C × 60s, (c) #3: 1100°C × 30s and (d) #4: 1200°C × 30s, respectively.

polished to a 1200 grit finish and then cleaned ultrasonically in acetone prior to joining.

A Ti–15Cu–15Ni(wt%) foil with 50 μm thickness (WESGO commercial product, with commercial name Ticuni foil) was used as the brazing filler metal. Ticuni is a clad-laminated brazing filler metal (LBFM) foil[18], whose solidus and liquidus temperatures are 910 and 960°C, respectively. The specimens, with Ticuni foil, were then carefully assembled into a sandwich type fixed by two graphite clamps and placed in the infrared furnace. A slight pressure was applied to keep all the parts in place by graphite screws during heating. Prior to the heating cycle, the infrared chamber was prevacuumized and then argon was purged for approximately 60 s. During heating, argon was continuously blown through the heating chamber at 200 ml/min. to minimize oxidation. The processing temperature was monitored with an R type Pt/Ir thermocouple fixed on the specimen's upper surface by graphite clamps.

The equipment for infrared joining used in this study was ULVAC SINKO-RIKO RHL-P610C type infrared gold image furnace. The maximum operating temperature was 1300°C. Four infrared heating conditions, (1)#1: 1150°C × 30 s, (2)#2: 1150°C × 60 s, (3)#3: 1100°C × 30 s and (4)#4: 1200°C × 30 s, were set and controlled by the EUROTHERM 818 type temperature controller. The heating rate of 3000°C/min. was adopted for all conditions. Figure 1 is the real temperature vs real time profile of sample #2 during the whole joining process which can be divided into four main stages: (I)heating, (II)dissolution, (III)isothermal solidification and (IV)cooling stages[19]. In Fig. 1, T_w, T_s and t_w are defined as the joining temperature, the solidus of Ticuni filler-metal and the programmer setting holding-time, respectively. Typically, 12 ~ 18 s is required for the specimen temperature to be raised to the set T_w temperature. Therefore, the real holding time for samples #1 ~ #4 was 16, 46, 48 and 12 s, respectively. Upon terminating the power, the specimen temperature dropped instantly since the furnace wall was not heated up by the infrared processing. Normally, the specimen cooled to below 500°C in about 90 s. From the T_w cooling to the T_s, the approximate cooling rate is about 1000°C/min estimated from Fig. 1. After joining, samples were cut, mounted and polished, and then etched with Kroll's reagent, which contained 2 ml HF, 4 ml HNO_3 and 100 ml H_2O, for SEM and EPMA examinations. Fractured surfaces of compressive shear-strength test were observed by SEM and EPMA and analyzed by X-ray diffraction (XRD).

Microstructures were observed by Nikon 104 OM and Philips 515 SEM. The JEOL JXA-8600SX EPMA was utilized to take the images, line-scanning profile (LSP) and quantitative composition of joined interface. The EPMA was operated at 15 KV

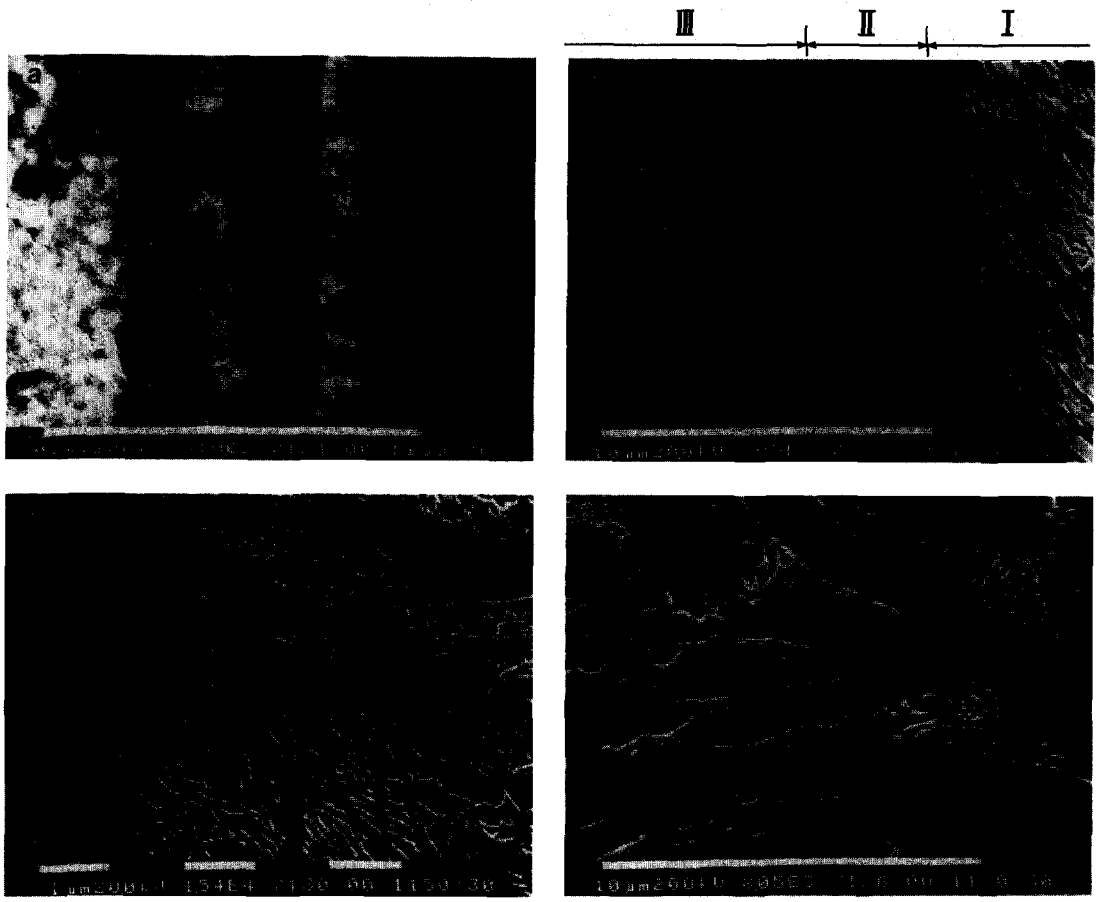

Fig. 4. The detailed SEM cross-section microstructures: (a) the entire joint interface, (b) the near-base metal side (Zones I & II), (c) the near-filler metal side of Zone III and (d) the near-base metal side of Zone III, of the joint interface of sample #1 which was joined at 1150°C × 30 s.

with a probe current 100 nA. XRD analysis with Cu Kα X-ray was conducted by using a Philips 1710 X-ray diffraction equipment carried out at 30 KV and 20 mA. The compressive shear-strength test was conducted at room temperature by Sintech 20/D instrument with the strain rate 0.25 mm/min.

3. EXPERIMENTAL RESULTS

3.1. Multilayered structures of joint zone

Figures 2(a)–(d) show the back-scattering electron images (BEIs) of joint interfaces for specimens #1 ~ #4, respectively. All the interfaces show different multilayered structures. These photos demonstrate that both T_w and t_w greatly affect the microstructural evolution. The brighter areas in Fig. 2 are Cu- and Ni-rich regions and the darker ones are Al-rich regions.

Figures 3(a)–(d) are the secondary electron images (SEIs) with Ti, Al, Cu and Ni EPMA line-scan profiles (LSPs) for samples #1 ~ #4, respectively. Obviously, Cu and Ni atoms are mainly concentrated in the central region and their concentrations decrease from inside to outside. On the contrary, Al concentration decreases from outside to inside. The variation of Ti concentration is rather minute and irregular.

The total thickness of joint interfaces increases from the original 50 μm to about 80 μm after infrared joining, indicating that some base-metal dissolved into the liquid filler-metal during joining processes. The thickness of the central zone (residual filler metal) is reduced as T_w and t_w increase. From Fig. 3, the LSPs curves vary continuously and smoothly in each layer, but there is a sharp and distinct compositional change at the interface between any two adjacent layers. This feature indicates that the microstructural evolution of joint interfaces is closely related to the isothermal solidification and subsequent solid-state interdiffusion between base-metal and liquid filler-metal at the T_w temperature.

3.2. Characteristic zones

Figures 4, 6 and 7 are the cross-sectioned microstructures of joints for samples #1 ~ #4, respectively. It is to be noted that small variations in T_w and t_w can cause significant changes in microstructural morphologies. Combined with the LSP results shown in Fig. 3, the overall cross-sectioned micro-

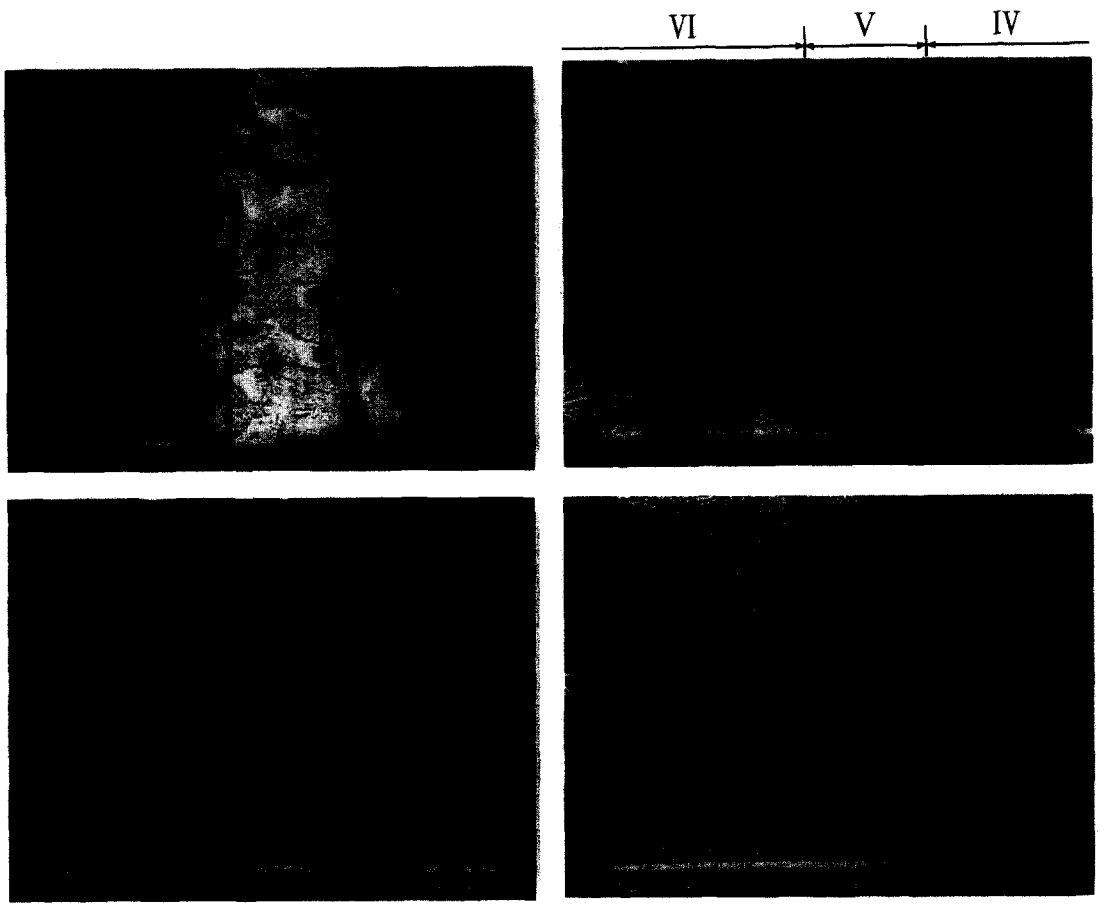

Fig. 5. The detailed SEM cross-section microstructures: (a) the entire joint interface, (b) the α_2-layer (Zone V) and its two sides, (c) the netted precipitation zone (Zone VI) and (d) the uniform but discontinuous precipitation zone (Zone IV), of the joint interface of sample #2 which was joined at 1150°C × 60 s.

structures of Figs 4–7 can be generalized into seven characteristic zones, as indicated in Fig. 8. They are named and described from outside to inside as follows:

(I) Zone I: The base-metal zone. This zone shows a pure γ-TiAl phase. Cracks shown in the photos are believed to be from the stress-induced corrosion cracking by reagent etching [20].

(II) Zone II: The base-metal interface. Its composition is similar to Zone I. Being a slender black layer near the base-metal, this zone is also a γ-TiAl area and no cracks can be revealed.

(III) Zone III: The columnar two-phase zone. This zone is the characteristic morphology of samples #1 and #4, and is composed of the black columnar strips and the white precipitation areas. The black strips show relatively rich Ti and Al content, but the white areas are Cu- and Ni-rich regions.

(IV) Zone IV: The discontinuous precipitation zone. This is one of the characteristic morphologies of samples #2 and #3, located between the α_2 layer (Zone V) and the base-metal (Zones I&II). In Zone IV, discontinuous white precipitations are of uniform distribution in sample #2, but are non-uniform in sample #3.

(V) Zone V: α_2 layer. This is also one of the characteristic morphologies of samples #2 and #3. It has been proven by EPMA that Zone V is the α_2-Ti_3Al phase with very little Cu and Ni content.

(VI) Zone VI: The netted precipitation zone. With high Cu and Ni content, the white precipitations in this zone have developed into an integral netted morphology.

(VII) Zone VII: The residual filler-metal zone. This is the central region of the joint interface with the highest Cu & Ni contents. This zone is a liquid phase before the cooling.

The insert table of Fig. 8 indicates that the above seven characteristic zones are not all coexisting in the same sample because the microstructure evolves as T_w and t_w vary. As shown qualitatively in Fig. 8, Zone III would change into Zones IV and V as the t_w is prolonged or T_w is decreased.

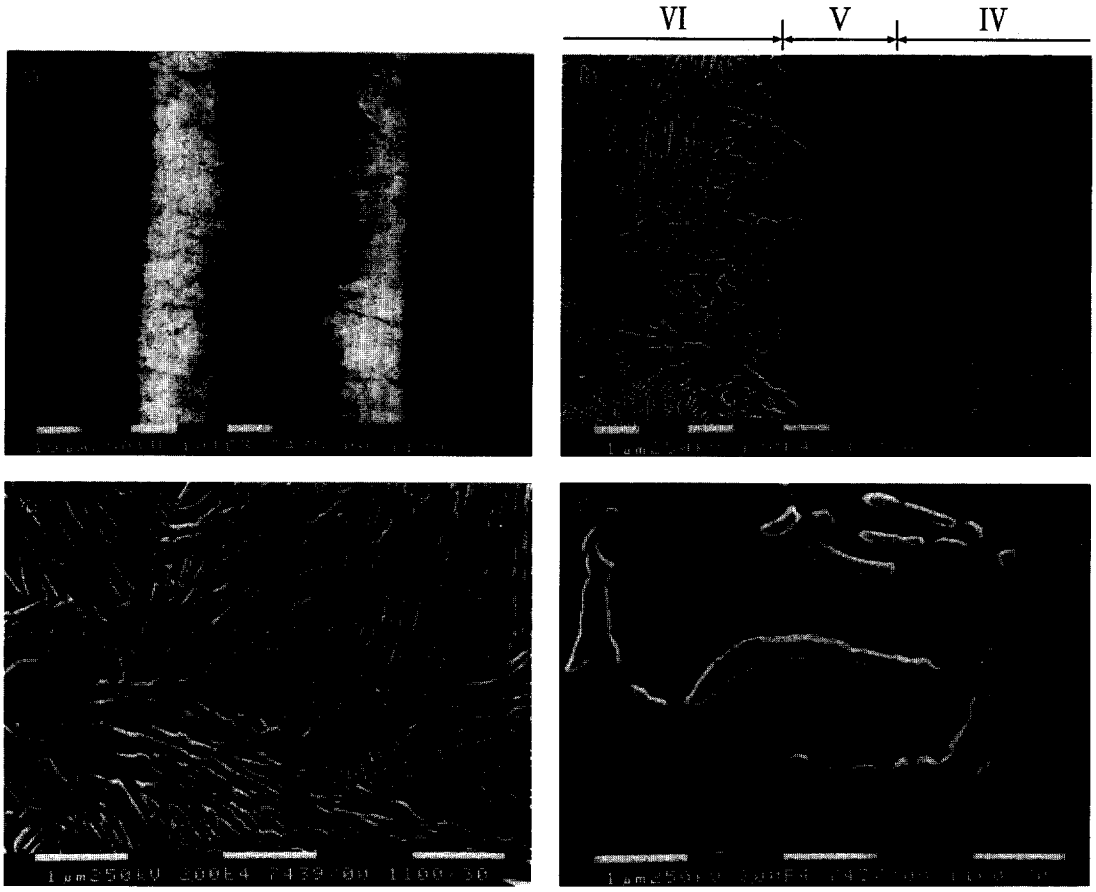

Fig. 6. The detailed SEM cross-section microstructures: (a) the entire joint interface, (b) the α_2-layer (Zone V) and its two sides, (c) the netted precipitation zone (Zone VI) and (d) the locally discontinuous precipitation zone (Zone IV), of the joint interface of sample #3 which was joined at 1100°C × 30 s.

4. DISCUSSIONS

4.1. The diffusion path and its corresponding high-temperature phases at 1150°C

The multilayered interfacial structures shown in Figs 4–7 are the consequence of atomic interdiffusion between base-metal and filler-metal [15–17]. The locus of the average composition of planes parallel to the original interfacial plane throughout the diffusion zone can be plotted on a ternary isotherm of Ti–Al–Ni (Cu is treated as Ni in this study) to establish the diffusion-path diagram [16, 17] of the joint. At high joining temperatures, as in this study, the volume diffusion will be the rate-limiting step with local equilibria existing at the interfaces [16]. Thus, the variations of constitutional phases in a joint interface can be displayed by comparing the diffusion-path diagram with the relevant ternary equilibrium phase diagram.

The diffusion path in the joint at T_w temperature can be estimated by the joint microstructures observed at room temperature if the cooling rate after joining occurs rapidly enough. This is because rapid cooling minimizes the interfacial concentration variation, which could be significant upon slow cooling [17]. In this study, due to rapid cooling ($\geqq$1000°C/min) from T_w to t_s, the joint interface does not have enough time to produce new compositional layers during cooling. Therefore, the observed room-temperature microstructures of Figs 4–7 are obtained from the cooling phase transformation of the high temperature phases formed at T_w. Under these circumstances, the diffusion path of the joint interface at T_w can be estimated by the room temperature microstructure and composition of each layer.

Figures 9(a) and (b) are the Ti–Al–Ni(Cu) pseudo-ternary diffusion paths for specimens #1 and #2 (T_w = 1150°C), respectively. In Fig. 9, it is assumed that Cu atoms behave similarly to Ni ones in the joint since both of them are β-Ti stabilizers and have similar atomic sizes and structures. In addition, Cu and Ni form an isomorphologic solid solution and show the complementary phenomena of their LSPs curves in Fig. 3. The Ni(Cu) values in Fig. 9 are obtained by adding the Ni and Cu contents together. By this Ti–Al–Ni(Cu) pseudo-ternary analysis, the diffusion paths of joint interfaces can be plotted, and the results can be further compared to the reported Ti–Al–Ni ternary phase diagram [21].

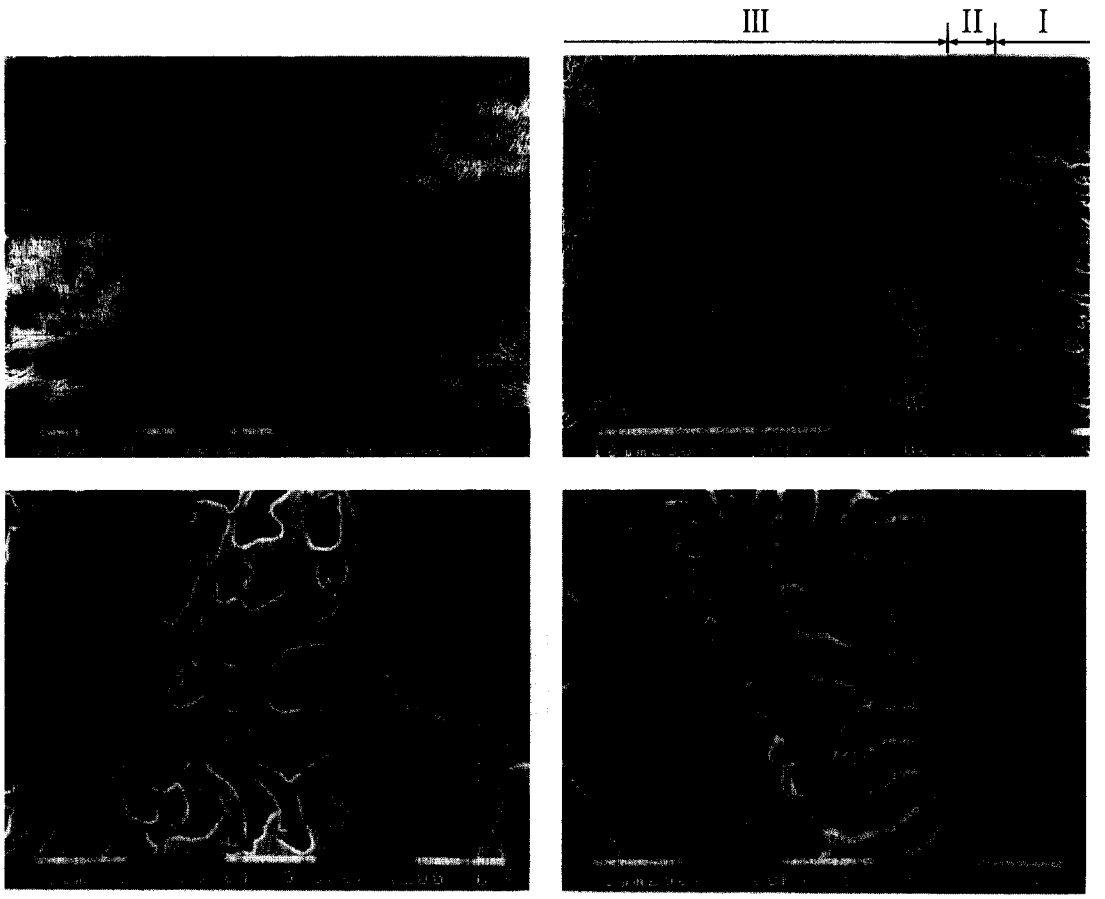

Fig. 7. The detailed SEM cross-section microstructures: (a) the entire joint interface, (b) the near-base metal side (Zone I and II), (c) the near-filler metal side of Zone III and (d) the near-base metal side of Zone III, of the joint interface of sample #4 which was joined at 1200°C × 30 s.

In Fig. 9, A and B are locus of the original base-metal and filler-metal compositions, respectively. I ~ VII express the composition regions of the seven characteristic interfacial zones described in Fig. 8. The composition locus of each zone is found to focus and vary smoothly in its own domain, but for each adjoining domain, the compositional diffusion path shows a large gap. According to the principle of multiphase diffusion in binary [15] or ternary [16, 17] solid-state systems, it is reasonable to suggest that each domain corresponds to one of the stable phases formed at the joining temperature T_w.

As mentioned above, the residual filler-metal zone (Zone VII) is the only liquid phase remaining in the joint before cooling. This feature can be easily proven by comparing the results of Fig. 9 with that of 1150°C Ti–Al–Ni isothermal phase diagram of Lee and Nash [21]. This comparison also implies that, at $T_w = 1150$°C, Zones I&II are both a γ-TiAl, Zone III is a two-phase mixed region, Zone IV is an α-Ti phase, Zone V is an α_2-Ti_3Al phase and Zone VI is a β-Ti phase.

It must be pointed out that the compositions of domains I, II, VI and VII are very close to the marked phases shown in the Lee and Nash diagram [21]. Thus, the phases of these zones at 1150°C can be directly identified by compositions they proposed. But concerning the other domains (III, IV and V), Fig. 9 shows that they deviate dramatically from those of the Lee and Nash diagram due to the absence of the α-Ti region in that diagram. Because the Lee and Nash diagram was evaluated from Liang's Ti–Al binary diagram [22], it was noted by the authors that there were considerable uncertainties in the referred to Ti–Al diagram. According to the more recent published Ti–Al binary diagram [2, 23], as shown in Fig. 10, there are indeed two α-Ti regions separated by an ordered α_2 phase at the 1150°C isotherm. Thus, the Lee and Nash diagram can not be directly used in the analysis of Zones III ~ V before it is appropriately modified. Drawings in Figs 9(a) and (b) were proposed following corrected phases suggested in Fig. 10.

From Fig. 9, it is clear that the atomic interdiffusion at $T_w = 1150$°C occurred through several intermediate phases. The diffusion paths are γ-TiAl/α-Ti/$\alpha + \beta$/β-Ti/residual liquid for sample #1 and γ-TiAl/α-Ti/α_2-Ti_3Al/β-Ti/residual liquid for sample #2. According to the multiphase diffusion theories, the diffusion path of an infinite couple on the ternary isotherm is defined uniquely only by its terminal

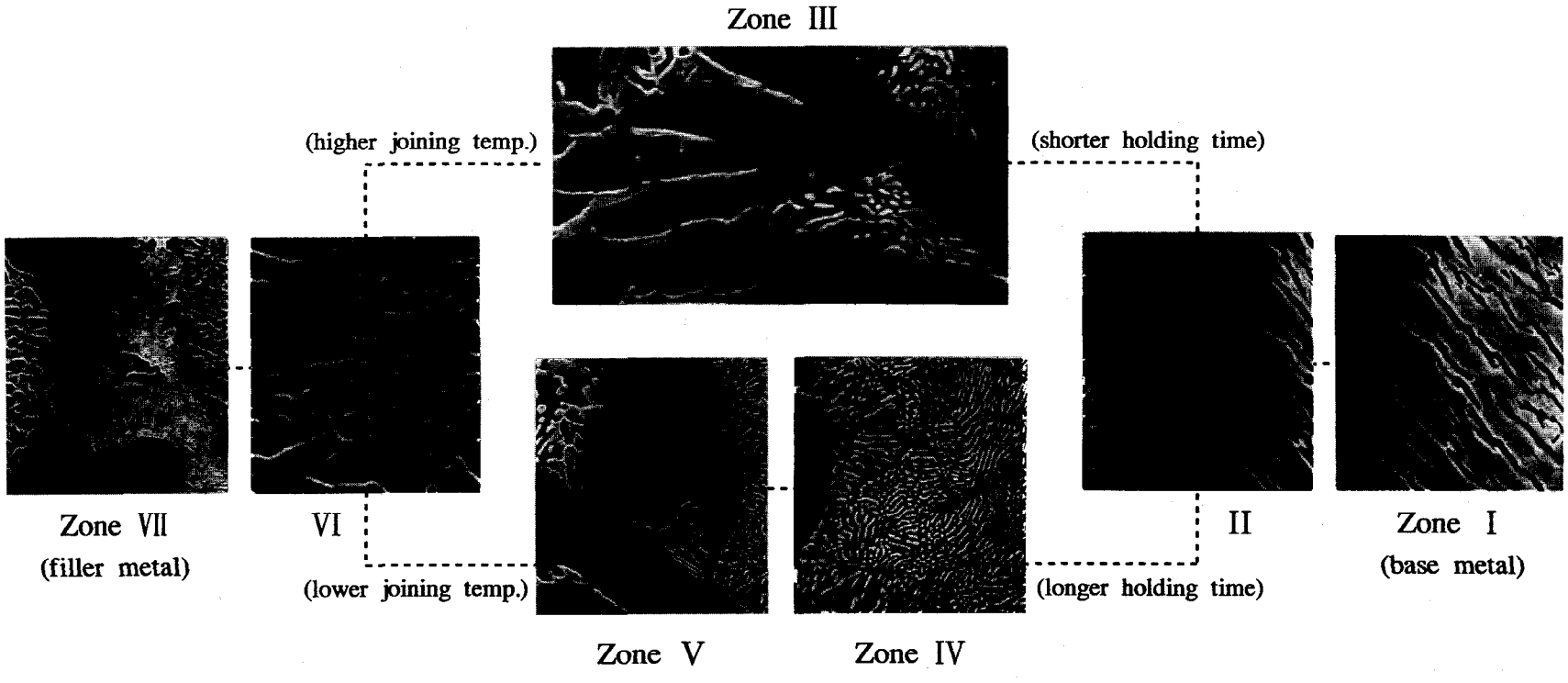

Zone No. / Sample No.	I	II	III	IV	V	VI	VII
#1: 1150℃×30sec.	○	○	○	×	×	○	○
#2: 1150℃×60sec.	○	○	×	○	○	○	○
#3: 1100℃×30sec.	○	○	×	○	○	○	○
#4: 1200℃×30sec.	○	○	○	×	×	○	○
Remark: ○: with and ×: without that specific characteristic zone.							

Fig. 8. The characteristic microstructures of seven zones of the overall cross-sectioned joint interfaces of the four joining conditions. The names and its characteristics for each zone are discussed in the text.

composition [17]. Thus, under thermodynamic consideration, the diffusion paths of infinite couples formed at the same T_w at all times should be time-invariant and behave as stationary lines. However, some kinetic factors may change the interfacial diffusion paths and produce different results, such as the finite couple [16], the moving terminus [17] and the delayed nucleation of some species [17], etc. These factors may cause the joint interfaces under different holding times to show non-consistent diffusion paths, as will be discussed below and in Part II of this study. For example, from Fig. 9, it is clear that the composition of residual liquid filler metal (one of the couple termini) changes with holding time from the original $Ti_{75}(Ni,Cu)_{25}$ (in at.%) to $Ti_{60}Al_{10}(Ni,Cu)_{30}$ at $t_w = 30$ s and then to $Ti_{45}Al_{25}(Ni,Cu)_{30}$ at $t_w = 60$ s. This continuous composition change of one terminus, called the moving terminus, is produced due to the finite couple effect of the filler metal and will change the driving forces of atomic interdiffusion and phase nucleation at T_w. Thus, the acquired diffusion paths and microstructures of samples joined at the same T_w change for different t_w.

Furthermore, as the holding time increases, the overall diffusion path obviously shifted to the Al-rich side while the Ni(Cu) content of the residual liquid phase increases from the original 25at.% to about 30at.%. According to the general qualitative trend proposed by Van Loo [16], these characteristics strongly point out that the inward diffusion of Al atom is the main control factor pertaining to the microstructural evolution of joint interfaces. One of the main purposes of Cu and Ni addition in the filler metal is to lower the melting point of the filler-metal [24]. However, these added Cu and Ni atoms change the interdiffusion system from a binary to a quaternary system, and therefore, cause more complex microstructures to evolve at the joining interface, as those shown in Figs 4–7.

By the same analytic procedures, the diffusion-path diagrams of samples #3 and #4 can be acquired. They are γ-TiAl/α_2 + X/α_2-Ti_3Al/β-Ti/residual liquid for sample #3 joined at 1100°C and γ-TiAl/α-Ti/α + β/β-Ti/residual liquid for sample #4 joined at 1200°C. Here, the X may be the λ-phase estimated by the detected composition locus of the corresponding area and reported on the 900°C Ti–Al–Ni isotherm [21]. The detailed time-dependent interfacial microstructural evolution at T_w and the effects of the joining temperature on the microstructural evolution at the joining interfaces will be further discussed in the part II of this study.

4.2. The phase-transformation during cooling from $T_w = 1150°C$

Upon terminating the power, the well-established high-temperature phases described in Section 4.1 will phase-transform to the room-temperature phases. Based on information presented in Figs 8 and 9, the correlation between the seven characteristic zones and their respective high-temperature phases can be obtained, as shown in Table 1. Because the acquired diffusion paths do not pass through any Ni(Cu)-base solid phase on the 1150°C Ti–Al–Ni(Cu) ternary isotherm, as will be discussed in Section 4.3, we suggest that all the white precipitates in the joint interfaces are merely formed by the cooling phase transformation. The proposed phase-transformation of each zone during the fast cooling are discussed as follows.

4.3. (1) Zones I & II: The base-metal zone and base-metal interface zone

After cooling, Zone I is a single γ-$Ti_{50}Al_{50}$ phase. From Fig. 10, the 1100°C/1200°C isotherm crosses the transus of γ-TiAl in Ti-rich side and this crossover is close to the composition of $Ti_{52}Al_{48}$. Thus, the composition of Zone II is suggested as $Ti_{52}Al_{48}$, as shown in Fig. 9(a) and (b). No cracks can be seen on Zone II because the stress relief may occur in this layer at T_w, as shown in Figs 4(b) and 7(b).

4.4. (2) Zone III: Columnar two-phase zone

Zone III, a typical two-phase mixed region shown in sample #1, is the cooling structure of the high-temperature columnar $\alpha + \beta$ two-phased zone. During rapid cooling, the columnar α-Ti directly transforms to the α_2-phase with no precipitation due to the similar composition of α-Ti and α_2 phases. At the same time, during cooling, the β-phase (the white precipitation area at T_{room}) also transforms to an α_2 phase with a considerable number of Ni(Cu)-rich precipitates due to its high Ni(Cu) content.

These white precipitations have been identified to be $TiCu_2$ and Ti(Ni,Cu) intermetallics by XRD analysis on the fractured surface of the compressive tested specimen, as will be discussed in Section 4.3. As shown in Figs 4(c) and 7(c), Zone III nearby the filler-metal side has a netted precipitation morphology due to this area containing higher Ni and Cu atoms and causing more precipitations after cooling. On the contrary, Zone III nearby the base metal side shows a discontinuous precipitation morphology due to its lower Ni and Cu contents, as shown in Figs 4(d) and 7(d).

4.5. (3) Zones IV and V: The discontinuous precipitation zone and α_2 layer

Zones IV and V simultaneously appear in the joint interface of sample #2 when Zone III vanishes due to the longer t_w, as shown in Figs 4 and 5. They are individually transformed from the α_2-Ti_3Al and the high Al% α-phase at T_w. Here, the high Al% α-phase is the α-phase located in between α_2-Ti_3Al and γ-TiAl phases at T_w (1150°C) isotherm, as shown in Fig. 10. Because α_2 is a stable phase at both T_w and T_{room}, it forms Zone V without any composition change during cooling. At the

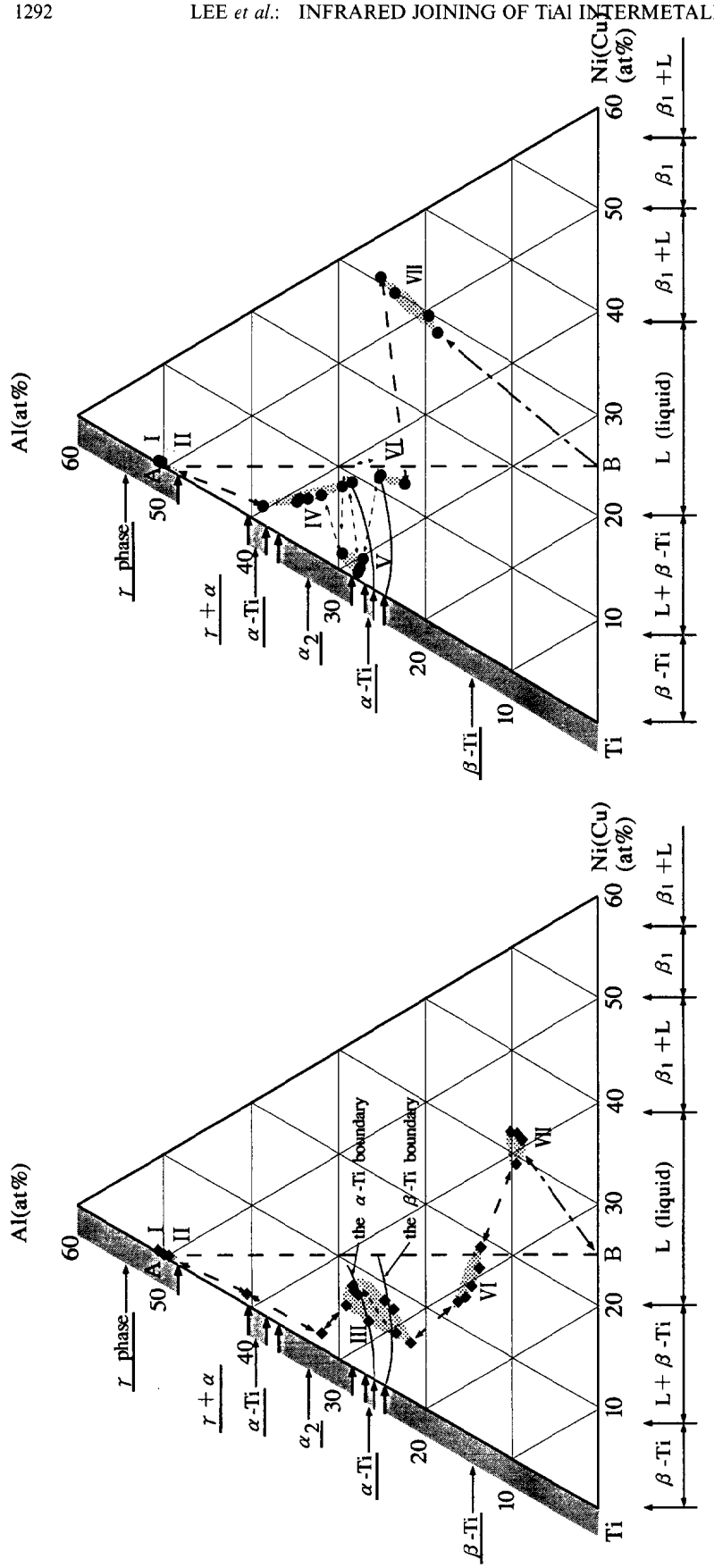

(a) #1: 1150°C×30sec. (b) #2: 1150°C×60sec.

A	Original base metal	III	Columnar two-phased zone	VI	Netted ppt. zone
I	Base metal zone	IV	Discontinuous ppt. zone	VII	Residual filler metal
II	Base metal interface	V	Continuous α_2-layer	B	Original filler metal

Fig. 9. The Ti–Al–Ni(Cu) pseudo-ternary diffusion path diagrams of joint interfaces, (a) for sample #1 joined at 1150°C × 30 s and (b) for sample #2 joined at 1150°C × 60 s, respectively. A, I ~ VII and B indicate the compositional loci of corresponding zone as shown in the table.

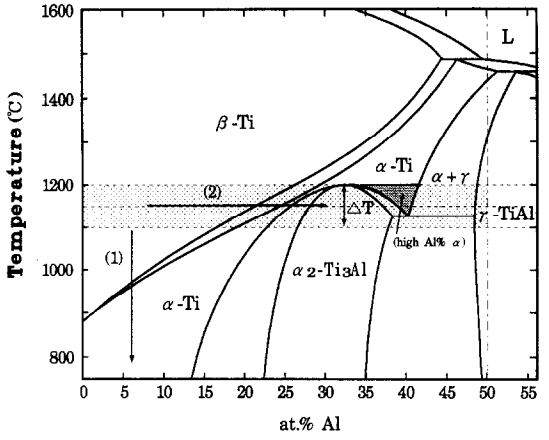

Ti-Al Phase Diagram

Fig. 10. The partial Ti–Al binary high temperature phase diagram [2, 23]. There are two types of β-Ti $\rightarrow$ α-Ti phase transformation produced by (1) cooling and (2) isothermal interdiffusion, respectively. Δ T is the α_2-phase supercooling of the specific joining temperature.

same time, the high Al% α-phase transforms to Zone IV. Jones *et al.* [25] reported that a Ti–Al alloy with Al $\geqq$ 45 at.% can form a full α_2-phase structure under a rapid cooling rate. In this study, we suggest that the disordered high Al% α-phase can transform to α_2 because its Al content is below 45%, as shown in Fig. 10. Besides, the high Al% α-phase can dissolve more Ni(Cu) atoms than its transformed ordered α_2-phase. Therefore, during the high Al% α transforms to α_2 phase in Zone IV, the excess dissolved Ni(Cu) atoms should be expelled from the fully ordered α_2 matrix and Ni(Cu)-rich precipitations will uniformly disperse in Zone IV, as shown in Fig. 5 of sample #2.

The microstructural evolution of Zone IV of sample #3 will be further discussed in the Part II. Because its joining temperature is at 1100°C, instead of 1150°C, the evolved phases and morphologies are different from those of Zone IV of sample #2.

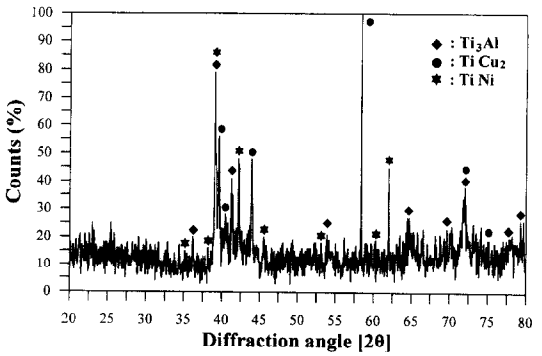

Fig. 11. The X-ray diffraction spectra for the fractured surface of the specimen joined at 1150°C × 60 s as sample #2. The X-ray diffraction pattern was interpreted according to the JCPDS cards [27].

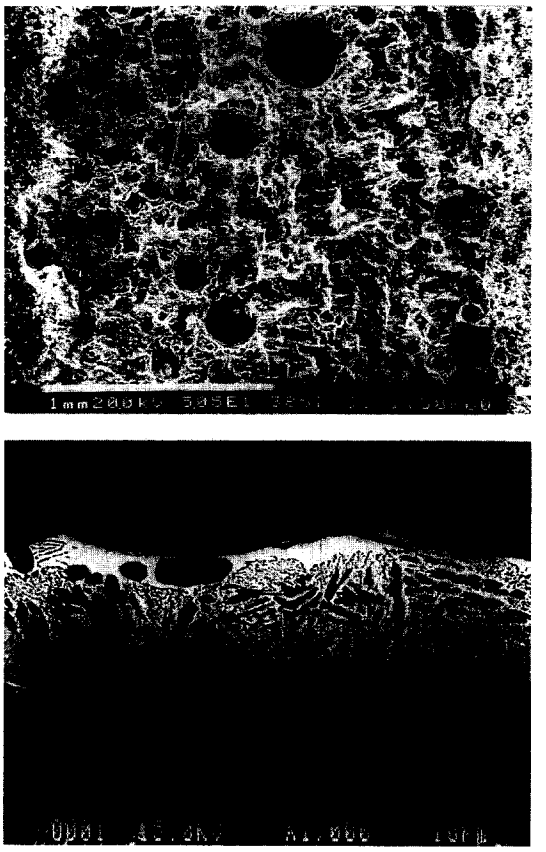

Fig. 12. (a) ~ (b) are the images of the fractured surface of Fig. 11 and the cross section of the same specimen, respectively.

4.6. (4) Zone VI: The netted precipitation zone

Zone VI corresponds to the region of the high-temperature β-Ti phase for both samples #1 and #2. Its room-temperature microstructure shows a unique morphology with a fully precipitated network due to its high Ni(Cu) content. This resulted from a ternary eutectoid reaction during cooling [26]. In our case, this reaction is identified to be β-Ti $\rightarrow$ α_2 + $TiCu_2$ + Ti(Ni,Cu) by the XRD analyses on the fractured surfaces of the specimen joined with the same condition as sample #2, as will be discussed in Section 4.3.

4.7. (5) Zone VII: The residual filler-metal zone

Zone VII is the region of the residual liquid filler metal at a high temperature. With low Al content, this region is the only area that still keeps the liquid state before cooling, and then solidifies as an eutectic morphology during the cooling. Due to the segregation during the isothermal solidification, this region contains higher Ni(Cu) content than the original filler metal.

Table 1. The phases and phase transformations of seven characteristic zones during fast cooling from $T_w = 1150°C$

Phases† at 1150°C)	γ-TiAl	$\beta+\alpha$		High Al%			Residual
		β-Ti	α-Ti	α-phase	α_2-Ti_3Al	β-Ti	liquid
Phases (at T_{room})	γ-TiAl	α_2-matrix + $TiCu_2$ + Ti(Ni,Cu)	Columnar α_2-Ti_3Al	α_2-matrix + Ni(Cu)-ppt	Isothermal α_2-Ti_3Al layer	α_2-matrix + $TiCu_2$ + Ti(Ni,Cu)	Rapid cooling phases
Zone No.‡	I II	III		IV	V	VI	VII

Remark: †These high-temperature phases are obtained from the diffusion diagrams of Fig. 9.
‡These zones are consistent with the observed room-temperature microstructures of Fig. 8.

4.8. The fractured surface of the joined interface

Compressive shear strength tests were carried out on specimens with the same joining conditions as samples #1 ~ #4. For specimens failing at the joining region, fractured surfaces were analyzed by XRD in order to identify the phases formed in the joint interface. Figure 11 shows the XRD spectra for the fractured surface of the specimen joined at 1150°C × 60 s (as sample #2). The Ti_3Al, $TiCu_2$ and Ti(Ni,Cu) are the major phases near the fractured surface, in which $TiCu_2$ and Ti(Ni,Cu) peaks have higher peak intensity than Ti_3Al one.

Figure 12(a) and (b) shows the images of the fractured surface and cross section of Fig. 11 specimen, respectively. From Fig. 12(b), the fracture has mainly taken place along Zone VII of joint interface. An EPMA test indicates that the spheres existing in Fig. 12(a) are $Ti_3Al(\alpha_2)$ phase. Combining the results of Figs 11 and 12, $TiCu_2$ and Ti(Ni,Cu) are the two major phases of those white precipitations existing in Zones III and VI. These observations agree well with the microstructural evolutions discussed in the previous sections.

5. CONCLUSIONS

Infrared joining of TiAl using Ti–15Cu–15Ni(wt%) foil as brazing filler metal was investigated at the temperature range of 1100°C ~ 1200°C for 30 ~ 60 s in a flowing argon environment. All the cross-sectioned microstructures at joint interfaces show distinct multilayered structures which were mainly formed by isothermal solidification and thereafter isothermal solid-state atomic interdiffusion. The diffusion of Al atoms from the TiAl base-metal into the joint zones at the joining temperature is the main controlling factor pertaining to the microstructural evolution of the joint interface. Seven characteristic zones can be distinguished in the joint. The corresponding high-temperature phases of these seven zones are γ-TiAl (I + II), $\alpha + \beta$ two-phase mixed (III), high Al% α-phase (IV), α_2-Ti_3Al(V), β-Ti (VI) and the residual liquid filler metal (VII), respectively. The locus of each specific zone shows a continuously or smoothly varying interval in the diffusion-path diagram and corresponds to one of the stable phases existing at the joining temperature. Experimental results show that the diffusion path of the joint interface at 1150°C for different holding times is: (a) held 30 s : γ-TiAl/α-Ti/α + β/β-Ti/residual liquid-phase and (b) held 60 s : γ-TiAl/high Al% α-phase/α_2-Ti_3Al/β-Ti/residual liquid-phase. On the Ti–Al–Ni(Cu) pseudo-ternary diffusion-path isotherm, the α-Ti, α_2-Ti_3Al and high Al% α phases are three distinguishable phases with their own compositional domains. The ordered α_2-Ti_3Al phase is surrounded by the entire α-base phase, just as it behaves in the binary Ti–Al phase diagram. The observed joint microstructures are obtained from the phase transformation of these well-established high-temperature phases through rapid cooling to room temperature.

Acknowledgements—The authors sincerely acknowledge the financial support of this research by the National Science Council (NSC), Republic of China, by the Grant NSC82-0405-E002-402.

REFERENCES

1. Kim, Y-W., *JOM*, 1989, **41**, 24.
2. Kim, Y-W. and Dimiduk, D. M., *JOM*, 1991, **43**, 40.
3. Yamaguchi, M. and Inui, H., in *Proc. Structural Intermetallics*, ed. R. Darolia, J. J. Lewandowski, C. T. Liu, P. L. Martin, D. B. Martin and M. V. Nathal. TMS, Warrendale, PA, 1993, p. 127.
4. Kim, Y-W., *JOM*, 1994, **46**, 30.
5. Patterson, R. A., Martin, P. L., Damkroger, B. K. and Christodoulou, L., *Welding J.*, 1990, **69**, 39s.
6. Baeslack III, W. A., Mascorella, T. J. and Kelly, T. J., *Welding J.*, 1989, **68**, 483s.
7. Mallory, L. C., Baeslack III, W. A. and Phillips, D., *J. Mater. Sci. Lett.*, 1994, **13**, 1061.
8. Nakao, Y., Shinozaki, K. and Hamada, M., *ISIJ International*, 1991, **31**, 1260.
9. Yan, P. and Wallach, E. R., *Intermetallics*, 1993, **1**, 83.
10. Cam, G., Bohm, K-H., Mullauer, J. and Kocak, M., *JOM*, 1996, **48**, 68.
11. Schwartz, M., in *Brazing*, 1st edn. Chapman & Hall, London, 1995, p. 1.
12. Annaji, S., Lin, R. Y. and Wu, S. K., in *Proc. Design Fundamentals High Temperature Composites, Intermetallics, and Metal-Ceramics Systems*, ed. R. Y. Lin, Y. A. Chang, R. G. Reddy and C. T. Liu. TMS, Warrendale, PA, 1995, p. 125.
13. Blue, C. A., Blue, R. A. and Lin, R. Y., *Scripta metall. mater.*, 1988, **32**, 127.
14. Singh, R., *J. appl. Phys.*, 1988, **63**, R59.
15. Reed-Hill, R. E., in *Physical Metallurgy Principles*, 2nd edn. Van Nostrand, New York, 1973, p. 559.
16. van Loo, F. J. J., *Prog. Solid St. Chem.*, 1990, **20**, 47.
17. Kirkaldy, J. S., in *Diffusion in the Condensed State*. London: Institute of Metals, 1987, p. 361.

18. Hoffman, K. F., Bird, R. K. and Dicus, D. L., *Welding J.*, 1995, **74**, 378s.
19. Zhou, Y., Gale, W. F. and North, T. H., *Int. Mat. Rev.*, 1995, **40**, 181.
20. Baeslack III, W. A., Mcquay, P. A., Lee, D. S. and Fletcher, E. D., *Mater. Char.*, 1993, **31**, 197.
21. Lee, K. J. and Nash, P., *J. of Phase Equilibria*, 1991, **12**, 551.
22. Liang, W. W., *Calphad*, 1983, **7**, 13.
23. McCullough, C., Valencia, J. J., Levi, C. G. and Mehrabian, R., *Acta metall. mater.*, 1989, **37**, 1321.
24. Rabinkin, A., Liebermann, H., Pounds, S. and Taylor, T., *Scripta metall. mater.*, 1991, **25**, 399.
25. Jones, S. A. and Kaufman, M. J., *Acta metall. metal.*, 1993, **41**, 387.
26. Den, L. C., Kao, P. W., Hsieh, K. C., Chang, S. F. and Lee, J. S., *Prakt. Metallogr.*, 1993, **30**, 567.
27. Cards, J. C. P. D. S., in *Joint Committee on Powder Diffraction Standards*. International Centre for Diffraction Data, Swarthmore, PA, 1990.